Electronic Supplementary Material (ESI) for Nanoscale.

Electronic Supplementary Information on: Photoassisted and multiphoton emission from single crystal diamond needle

M. Borz,[1] M.H. Mammez,[1] I. Blum,[1] J. Houard,[1] G. Da Costa,[1] F. Delaroche,[1] S. Idlahcen,[2] A. Haboucha,[2] A. Hideur,[2] V.I. Kleshch,[3] A.N. Obraztsov,[3,4] and A. Vella[1,*]

[1] *Groupe de Physique des Matériaux UMR CNRS 6634, Normandie Université, Université-INSA de Rouen, Avenue de l'Université BP 12, 76801 Saint Etienne du Rouvray, France*

[2] *CORIA UMR CNRS 6614, Normandie Université, Université-INSA de Rouen, Avenue de l'Université BP 12, 76801 Saint Etienne du Rouvray, France*

[3] *M. V. Lomonosov Moscow State University, Department of Physics, Moscow 119991, Russia.*

[4] *University of Eastern Finland, Department of Physics and Mathematics, Joensuu 80101, Finland.*

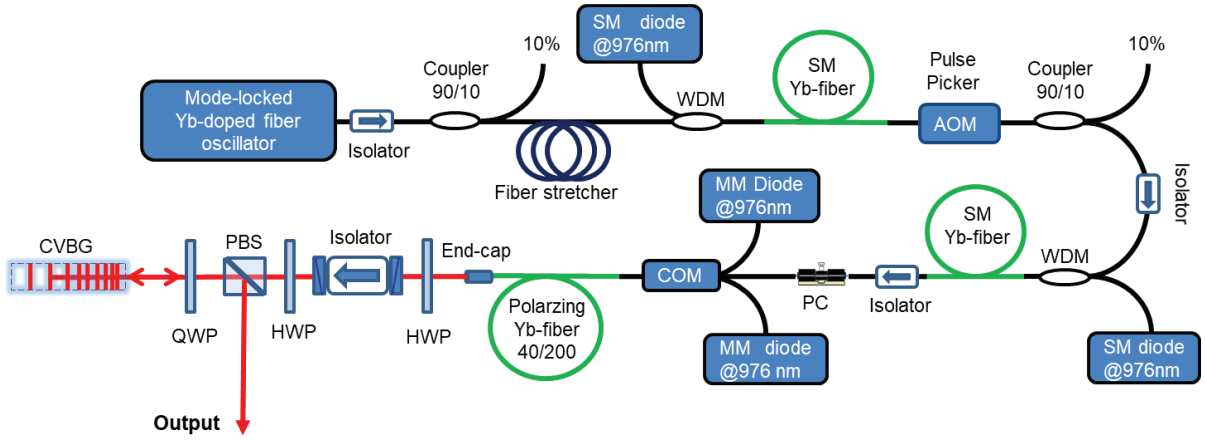

FIG. 1: Experimental set-up of the fiber-based chirped-pulse amplifier system. WDM : Wavelength-division-multiplexer; COM : pump and signal fiber combiner; PBS : polarization beam splitter; CVBG : chirped volume Bragg grating; PC : polarization controller; QWP : quarter waveplate; HWP : half waveplate.

S1. LASER SYSTEM

The schematic diagram of the laser system used to drive this experiments is shown in Fig. 1. The pump laser was a 3 μJ class ultrafast ytterbium-doped fiber-based chirped-pulse amplifier system operating at 1040 nm. The system is seeded by a home-made all-fiber oscillator operating in the dispersion-managed soliton regime and delivering a stable pulse train at 18 MHz repetition rate. A fiber Bragg-grating is used for intra-cavity dispersion management. This SESAM-based mode-locked laser provides a typical parabolic shaped spectrum with pre-chirped pulses of 9 ps duration and 15 nm spectral width (see Fig. 2. The output autocorrelation measured using a second harmonic generation-based autocorrelator is given in the inset of Fig. 2. The autocorrelation is well fitted assuming a Gaussian pulse shape with 9.2 ps width (FWHM : full-width at half maximum). Fig. 2(b) shows the radiofrequency (rf) spectrum of the signal in 400 kHz span. The rf spectrum of intermode beat notes presents an excellent signal-to-noise ratio of >75 dB. It exhibits only one noise substructure at low frequencies (<5 kHz). The amplitude fluctuations associated to this sub-structure are lower than 0.4 % rms. The seed pulses were further stretched to approximately 250 ps by means of a long passive fiber. To access the high energy regime, a fiberized acousto-optical modulator (AOM) was placed prior to the main power amplifier in order

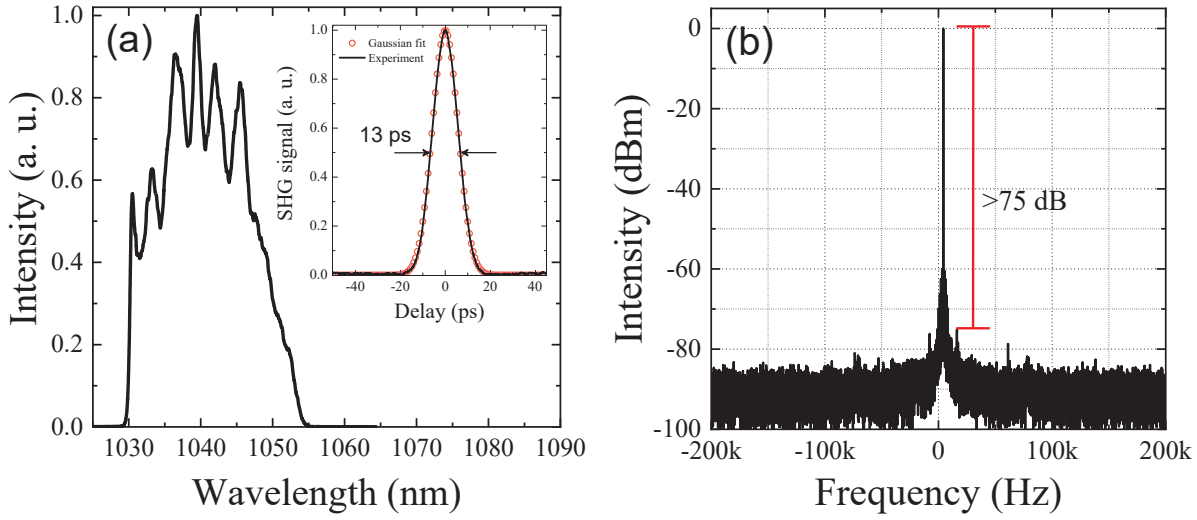

FIG. 2: Mode-locked Yb-fiber seed oscillator outputs : (a) Optical spectrum and autocorrelation (Inset) and radiofrequency spectrum at 400 kHz span and 20 Hz resolution bandwidth (b)

to lower the fundamental repetition rate down to 900 kHz. Two core-pumped Yb-doped fiber preamplifiers were used to compensate the losses in the stretcher and AOM. The power amplifier is based on a cladding-pumped heavily ytterbium-doped polarizing large mode area microstructured fiber with 40 μm core diameter and 200 μm pump cladding. The pump and signal are coupled into the gain fiber through a fiber combiner thus offering a highly integrated laser configuration. A polarization controller is used to match the beam polarisation with the LMA gain fiber polarization axis thus ensuring a linearly-polarized amplified pulses. The amplified pulses are then dechirped in a chirped volume Bragg grating compressor to less than 600 fs duration. We note that the residual pump is removed using a dichroic mirror which is not shown in Fig. 1. The FCPA system performances remains very stable for repetition rates lying between 0.9 to 18 MHz with a maximum output power of 2.5 W which corresponds to more than 2.7 μJ. The laser outputs for an average power of 2 W and different repetition rates are depicted on Fig. 3. We note that the amplified pulses suffer from gain narrowing within the amplification stages as well as from some spectral clipping at short wavelengths. The output spectral width is lower than 8 nm. So, the output pulse durations varied between 500 and 700 fs when decreasing the repetition rate from 18 to 0.9 MHz (see Fig. 3). The pulse-to-pulse amplitude fluctuations measured at the amplifier output remains lower than 1 % rms. To reach even lower repetition rates, a free-space AOM

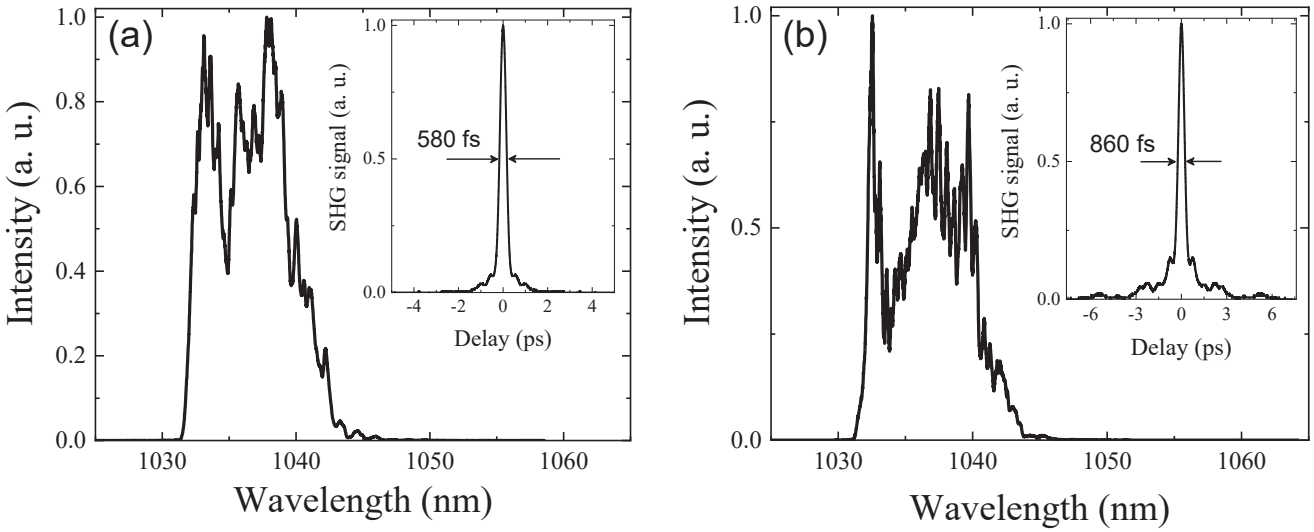

FIG. 3: Amplifier outputs at an average power of 2 W for 18 MHz (a) and 900 KHz (b) repetition rates. Insets correspond to the measured autocorrelation traces.

is included at the laser output. The contrast measured at the laser output is higher than 10.000 thus limiting the impact of interpulse residual noise.

S2. CURRENT MEASUREMENT

In order to measure the emission current using CCD recorded images we proceeded as follows: first we eliminated the noise by ignoring the regions of the image that recorded an intensity below 20 units, over a total range of 256. Two images obtained for a laser assisted emission from a diamond tip at $I_{peak} = 27$ GW/cm^2 and $V_{tip} = 100$ V and 280 V are reported in Fig. 4 (a) and (b), respectively.

Several spots of different sizes are visible. The number of spots (N_{spots}) was counted using a routine that determined the position of local intensity maxima, each maximum corresponding to a spot. The current is calculated by : I=$\frac{eN_{spots}}{t_{image}}$, where t_{image} is the acquisition time of the CCD and e is the elemental charge.

One can notice that the different spots can have different intensities. This can be due to the natural distribution of spot intensities inherent to the functionning of MCP based detectors. But it is also possible that for large number of counts on a single image, some high intensity spots might actually correspond to multiple spots that are too close to each other to be discriminated. This effect would cause the measured number of counts to be

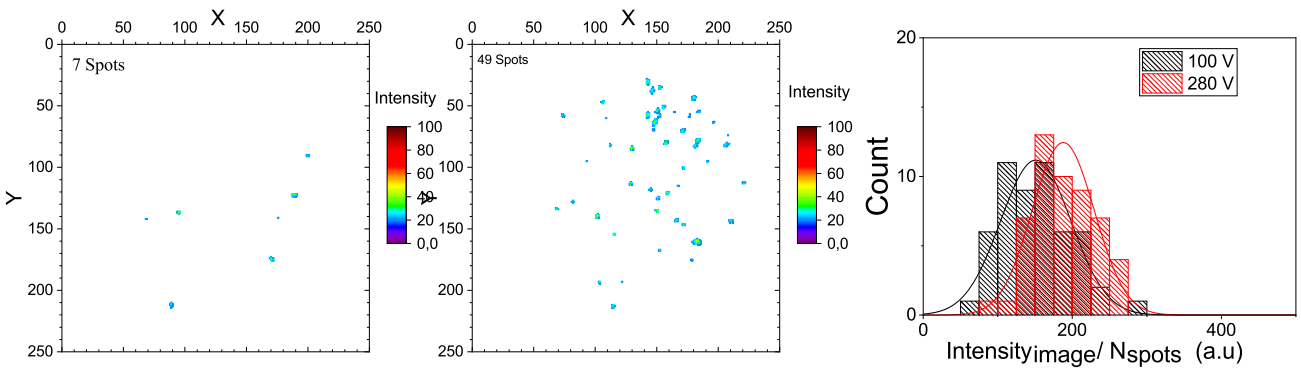

(a) (b) (c)

FIG. 4: Electron hitmap as imaged by the CCD camera. Only the signal with an intensity above 20 over 256 is displayed. The laser intensity is 27 GW/cm^2 and the applied voltage is $V_{tip} = 100$V (a) and $V_{tip} = 280$V (b). The acquisition time is 10 ms per image.(c) Distribution of the ratio $\frac{Intensity_{image}}{N_{spots}}$ for all the images recorded in the two experimental conditions of (a) and (b)

underestimated at high currents. However, even if two spots are not discriminated, they should still both contribute to the total image intensity, and thus this should reflect on the value of the average intensity per spot. In order to quantify this effect, we calculated the distribution of the ratio: $\frac{Intensity_{image}}{N_{spots}}$ for all the images recorded in the two experimental conditions of Fig. 4 (a) and (b), which corresponds to a current of 10^3 and 10^4 count·s^{-1}, respectively. The maximum of the distribution shifts towards higher values when the applied voltage increases(see Fig. 4(c)). An increase of about 20% was calculated for the images of Fig. 4. This means that the number of detected spots is underestimated of about 20% at highest emission currents.

S4. ESTIMATION OF NUMBER OF PHOTON FROM FN PLOTS.

At high voltages ($V_{tip} > 300$ V and $\frac{1}{V_{tip}} < 0.0033$ V^{-1}), the slope of the $I - V_{tip}$ lines (in FN coordinates) decreases when the laser power is increased. The step by step decrease of the FN slope is reported in Fig .5. This behavior can be explained by the gradual increase in the number of absorbed photons.

From the value of the slope of the F.N plot without illumination, we calculate the value

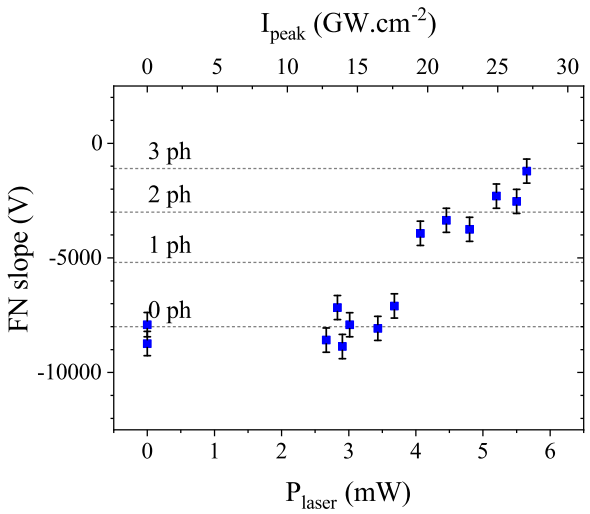

FIG. 5: Slope of the FN plots as a function of laser power (P_{laser}) (bottom abscissa) or laser intensity I_{peak} (top abscissa). Dashed lines correspond to the slopes of the FN plots calculated taking into account the reduction of the barrier height by the absorption of one, two or three photons.

of the slope of the F.N. plot when the effective barrier height is reduced by 1.2 eV(2.4 or 3.6 eV) by the absorption of one (two or three) photon, respectively. These values are reported as dashed lines in Figure S5.

S5. MEASUREMENT OF THE ENERGY-SELECTIVE LASER-POWER DEPENDENCE OF PEAKS FROM ENERGY SPECTRA.

In order to confirm this emission mechanism, an energy-selective, laser-power dependence measurement was performed on the peaks of energy spectra reported in Fig. 7a in the main text. This measurement is shown in Fig. 6, in log scale. Each line corresponds to one peak of the photoelectron spectra as defined in Fig. 7b, where the electron yield is obtained by integrating the spectra over the energy window corresponding to each peak (e.g. for the first peak, the energy rangies from 2.4 to 3.6 eV).

The power factor varies from 2.8±0.6 for the first peak, to 5.7±1.4 for the last peak, where the error bars correspond to the fitting uncertainty. As expected for multi-photon emission, each peak corresponds to a different number of absorbed photons, therefore corresponding to a different exponent. The exponent of the first peak is close to 3, suggesting that the

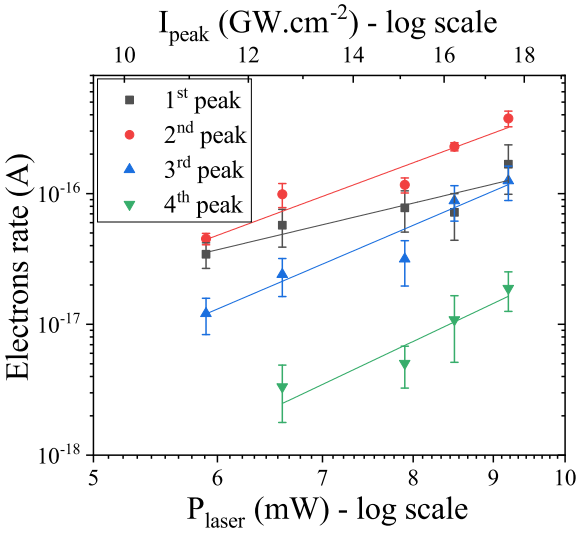

FIG. 6: Log-log plot of electron yield versus laser intensity plotted for each peak of the energy spectra of Fig 7(a) in the main text. The dots are the experimental values, and the lines correspond to the least square fits from which the exponent is extracted.

effective work function of our diamond needle at $V_{tip} = 100$ V is roughly equal to 3 times the photon energy (ϕ_{eff} =3.6 eV).

The second peak has an exponents of 4.4 ± 0.6, corresponding to the absorption of 4 photons and the third peak of 5.1 ± 0.7, associated to a 5 photons process. The last peak can be isolated from the background noise only for the higher values of the laser power; therefore the error bar associated to the exponent of this peak is larger: 5.7 ± 1.4, showing that at high laser intensity the system absorbs 6 photons before electrons leave the diamond needle. Since the emission is very sensitive to the increase in the laser intensity (a small increase in laser intensity is enough to reach the maximum current that can be measured with the detection system. Hence, in order to avoid the saturation of our detection system, we explore a limited range of laser power, therefore the value of the exponent presented here can be affected by a larger error.